ACS APPLIED MATERIALS & INTERFACES

Research Article

www.acsami.org

Sulfur-Doped Molybdenum Oxide Anode Interface Layer for Organic Solar Cell Application

Pingli Qin,[†,‡] Guojia Fang,*[,†] Fei Cheng,[†] Weijun Ke,[†] Hongwei Lei,[†] Haoning Wang,[†] and Xingzhong Zhao*[,†]

[†]Key Laboratory of Artificial Micro- and Nanostructures of Ministry of Education of China, Department of Electronic Science and Technology, School of Physics and Technology, Wuhan University, Wuhan, Hubei 430072, P. R. China

[‡]School of Science, Wuhan Institute of Technology, Wuhan, Hubei 430073, P. R. China

ABSTRACT: Efficient organic solar cells (OSCs) based on regioregular of poly (3-hexylthiophene):fullerene derivative [6,6]-phenyl-C_{61}butyric acid methyl ester composites have been fabricated on indium tin oxide (ITO) coated glass substrates by using a sputtered sulfur-doped molybdenum oxide (S-MoO_3) film as anode interface layer (AIL). With the help of X-ray photoelectron spectroscopy and ultraviolet photoelectron spectroscopy, we find that oxygen flow ratio control can modulate the amount of sulfur doping into MoO_3, then further tune the $Mo^{+4}/Mo^{+5}/Mo^{+6}$ composition ratios, Fermi level, electron affinity, valence band ionization energy and band gap of MoO_3. A partially occupied Mo 4d-bands of Mo^{5+} and Mo^{4+} states modulated by sulfur doping are the main factor which influences the valence electronic structure of S-MoO_3.These orbitals overlap interrelation push the valence band close to S-MoO_3's Fermi level, thus make it into a p-type semiconductor. S-MoO_3 with smaller ionization energy and electron affinity is better suitable as an efficient AIL. On the basis of these AILs, a photovoltaic power conversion efficiency up to 3.69% has been achieved, which is 12% higher than that in pure MoO_3 AIL case. The result thus shows that sulfur doping is a useful method to modify anode interface layer for improving the hole-transport properties of MoO_3, which can improve the device performances.

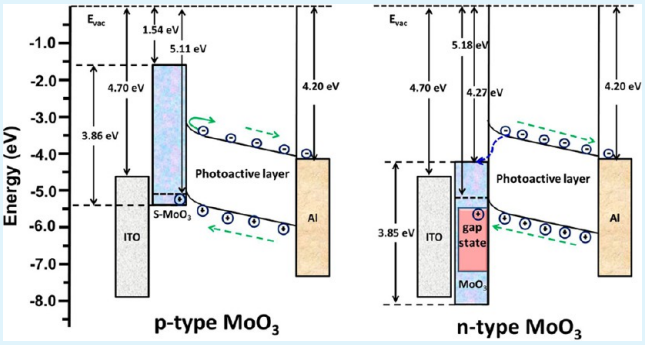

KEYWORDS: *MoO_3, sulfur doping, work function, anode interface layer, organic solar cell*

Organic solar cells (OSCs) based on blends of conjugated polymers and fullerene derivatives have attracted much attention in the past two decades because of their potential as low-cost, lightweight, and large-area flexible photovoltaic devices.[1,2] The rapid progress in the organic photovoltaic field has made OSC a viable source of renewable energy, as power conversion efficiencies (PCEs) exceeding 10% have been reported.[3] A vast number of studies involve a blend of regioregular poly (3-hexylthiophene) (P3HT) and [6, 6]-phenyl-C_{61}-butyric acid methyl ester (PCBM) for which solar cell efficiencies up to ~5.0% have been realized.[4] Traditional OSC is composed of a transparent anode, an anode interface layer (AIL), a photoactive layer (PAL), and a top cathode. AIL must have high optical transparency, good chemical stability, a large ionization potential, and good electron blocking capability.[5] In the conventional solar cell, poly (3, 4-ethylene-dioxythiophene):poly (styrene-sulfonate) (PEDOT:PSS) is used as AIL to smooth the surface and modulate work function (WF) of the indium tin oxide (ITO) anode.[2,6] However, PEDOT:PSS has been shown to have acidic nature, which results in degradation mechanisms and reduces device stability.[7] Therefore, efforts to replace PEDOT:PSS with transition metal oxide semiconductors, such as nickel oxide,[5,8] molybdenum oxide (MoO_x),[2,9−11] vanadium oxide,[9,12] chromium oxide,[13] and tungsten oxide,[14−16] are currently received increasing attention in OSC.

Among the metal oxide AILs used in OSCs, MoO_3 is a promising candidate because of its relatively good hole-mobility, environmental stability, and transparency. But the underlying physical mechanisms pertaining to their electronic structure remain somewhat undefined. MoO_x thin films had initially been considered to have the valence band edge at 5.4 eV,[9−11] the conduction band edge at 2.3 eV,[17] and a WF of 5.2 eV,[18] indicating MoO_3 has a p-type conductive mechanism. However, when evaporated, MoO_3 possesses a Fermi level that is pinned at 6.86 eV, an electron affinity (EA) of 6.70 eV, and ionization energy (IE) of 9.68 eV,[19] which indicates that it is an n-type material. And the high EA enables the highest occupied molecular orbital (HOMO) of many organic semiconductors to possess a sufficient density of states overlap with the empty MoO_3 conduction band states to allow the ground state hole-charge of organic semiconductor transferring to MoO_3,

Received: December 4, 2013
Accepted: February 7, 2014
Published: February 7, 2014

   dx.doi.org/10.1021/am405571a | *ACS Appl. Mater. Interfaces* 2014, 6, 2963−2973

rendering it p-doped.[20,21] Moreover, the local electron depletion of the donor and acceptor phases at the interface would in principle act to reduce back-contact recombination of the electrons from fullerene acceptors, while improving hole-collection from the donor materials at this interface. Such a situation may explain why n-type MoO_3 modified anodes have been so successfully used as a AIL in OSCs.[22,23] Because of the significantly deeper valence band edge of MoO_x, Wong's group[24] considered that holes are not transported to ITO through the valence band of MoO_x. Instead, holes are transported from the MoO_x/organic interface to ITO through MoO_x gap states. This hole-selective behavior can be explained by invoking band bending at the MoO_x/organic interface which could partially block electrons. Therefore, an n-type semiconductor is not a good AIL, and a p-type semiconductor is an essential but not necessary requirement for AIL.

Hole-mobility is typically much lower than that of electron in OSC. It is thus very important to let hole transport smoothly through the AIL and its related interfaces effectively for improving the efficiency of OSC. MoO_x film is a multivalent complex with Mo^{6+}, Mo^{5+}, and Mo^{4+} oxidation states.[19,24] And many defects (especially surface defects) in the multivalent complex could have very strong adsorption properties of water and oxygen, which is not beneficial to the stability of OSC. Therefore, many research groups have tried to improve the hole-mobility and stability of the inorganic oxide AIL from every aspect. Aside from various fabrication methods, such as thermal evaporation,[9,11] sol−gel method,[25−27] and sputtering deposition,[28] being employed to prepare the AILs, some groups attempt to increase the electrical conductivity of AIL by inserting a thin metal and make AIL into a sandwich structure without sacrificing their transmittance.[29−31] And Shao et al. used a blend of MoO_3 and PEDOT:PSS as AIL to improve PCE and stability of OSC.[32] Moreover, Ghosh's[33] and Fang's[28] groups exploited the treatment of the metal oxide AIL surface by plasma and ultraviolet (UV) ozone treatment to reduce the surface defect of AIL film and to make better AIL contact with PAL, respectively.

At the same time, it is also found that by nitrogen doping of amorphous chromium oxide (ACO) AIL, water dissociation and hydroxylation on ACO surface can be prevented, and thus improved hole-mobility and stability of OSC.[13,34] This provides an enlightenment for us to regulate the constituents of molybdenum oxidation states in the film by doping, and then to further adjust its energy level, and make it match the polymer (or the anode) energy level well, which could effectively reduce the surface defects and form S−Mo−S band[35,36] to improve the mobility of charge carrier in the MoO_x film.

Although n-type MoO_x has been successfully used as AIL of OSCs, hole recombination occurs inevitably in the MoO_x/organic interface due to smaller band bending potential barrier at the interface. If p-type MoO_x can be obtained, carrier recombination at the interface can be effectively blocked. The fabrication of p-type semi-conductive sulfur doped MoO_3 films (S-MoO_3) and its application as AIL of OSC are seldom reported. In this paper, we report the fabrication and characterization of OSCs based on S-MoO_3 as AIL by the radio frequency (RF) magnetron sputtering method. Transparent S-MoO_3 films have been fabricated in different oxygen flow ratio $f(O_2)$ (O_2/(O_2+Ar)) on ITO and glass sheet substrates. PCE of OSCs largely depends on $f(O_2)$, and OSC with S-MoO_3 shows 12% improvement in PCE compared to that in the device with MoO_3 only AIL.

EXPERIMENTAL SECTION

S-MoO_3 films were prepared by a RF magnetron sputtering system using a ceramic MoS_2 (99.9% pure) target in Ar and O_2 atmosphere. The chamber pressure was pumped down to $<3 \times 10^{-4}$ Pa and backfilled with the sputtering gas to a pressure of 1.0 Pa. The ITO and glass sheet substrates were cleaned with successive rinses in ultrasonic baths of acetone, ethanol, and deionized water and blown with dry N_2 before deposition. Both high-purity Ar (99.999% pure) flow rate and O_2 (99.999% pure) flow rate were modulated by mass-flow controllers during deposition. Mixtures of Ar and O_2 with different $f(O_2)$ of 0, 5, 10, 20, 30, and 40% were introduced into chamber by mass-flow controllers during deposition. The total gas flow rate retained at 10 sccm. The substrate temperatures were kept at 423 K because the decline of ITO photoelectric properties resulted from higher substrate temperature. Pre-sputtering was performed to obtain a steady-state sputtering condition. The deposition rate (~0.5 Å/s) as well as the nominal film thickness was monitored with a quartz crystal thickness monitor (TM-400, Maxtek, USA). Using a surface profilometer (FTS2-S4C-3D, Taylor Hobson, UK), we checked the film thicknesses and obtained good agreement. The distance between the target and the substrate was about 7 cm and the target was located beneath the substrates. The deposition power was kept at 40 W and the thickness of the films was controlled by the sputtering time. A reference solar cell with ca. 10 nm MoO_3 as AILs was fabricated, which was deposited according to the parameters in the reference.[37]

X-ray photoelectron spectroscopy (XPS) and ultraviolet photoelectron spectroscopy (UPS) were performed using a XPS/UPS system (Thermo Scientific, ESCLAB 250Xi, USA). All the films were sputtering-cleaned to remove atmospheric contamination in the XPS chamber for approximately 20 s by lower energy of Ar^+, and the Ar^+ gun was operated at 0.5 kV at a pressure of 1×10^{-7} Pa. The vacuum pressure of the analysis chamber was better than 2×10^{-8} Pa. For XPS, survey scans to identify overall surface composition and chemical states were performed using a monochromated Al Kα X-ray source ($h\nu$ = 1486.68 eV), detecting photoelectrons at 150 eV pass energy and a channel width of 500 meV. High-resolution scans to identify bonding states were performed at 20 eV pass energy and 50 meV channel width. The surface carbon signal at 284.6 eV was used as an internal standard. UPS was carried out using He I radiation at 21.22 eV from a discharge lamp operated at 90 W, a pass energy of 10 eV, and a channel width of 25 meV. Conductive, grounded samples were run without charge compensation. A −9 V bias was applied to the samples in order to separate the sample and analyzer low-kinetic-energy cutoffs. The transmittance of the S-MoO_3 films was measured by a UV−Vis−NIR spectrophotometer (CARY5000, Varian) in the 200−800 nm wavelength range at RT. The morphology of the S-MoO_3 films was characterized by atomic force microscopy (AFM SPM-9500J3, Shimadzu, Japan) with the contact mode (scanning tip: single-crystal Si_3N_4, spring constant: 0.02 N m^{-1}).

Regioregular P3HT (Rieke Metals, Inc.) and PCBM (Nano-C) were used for PAL. Thin film OSCs were prepared by the blends of P3HT:PCBM (1:1 by weight) in chlorobenzene. The devices were prepared on ITO glass (R_{sheet} = 10 Ω/sq) substrate. S-MoO_3 films were then deposited by RF sputtering. Subsequently, the blends were deposited through spin-casting at 1000 rpm at room temperature for 30 s. Finally Al electrode was deposited via thermal evaporation with approximately 100 nm thick and the whole device was annealed at 423 K for 7 min. The active layer is 0.1 cm^2. Photovoltaic measurement was conducted illuminating the devices under a solar simulator with AM1.5G filter. The illuminated current density−voltage (J−V) characteristics of the OSCs were examined using a Keithley 2400 sourcemeter. The simulated light intensity was adjusted to 100 mW/cm^2 calibrated with a Thorlabs optical power meter. The corresponding incident photo-current efficiency (IPCE) spectrum was measured with a QE/IPCE Measurement Kit system (Newport, USA).

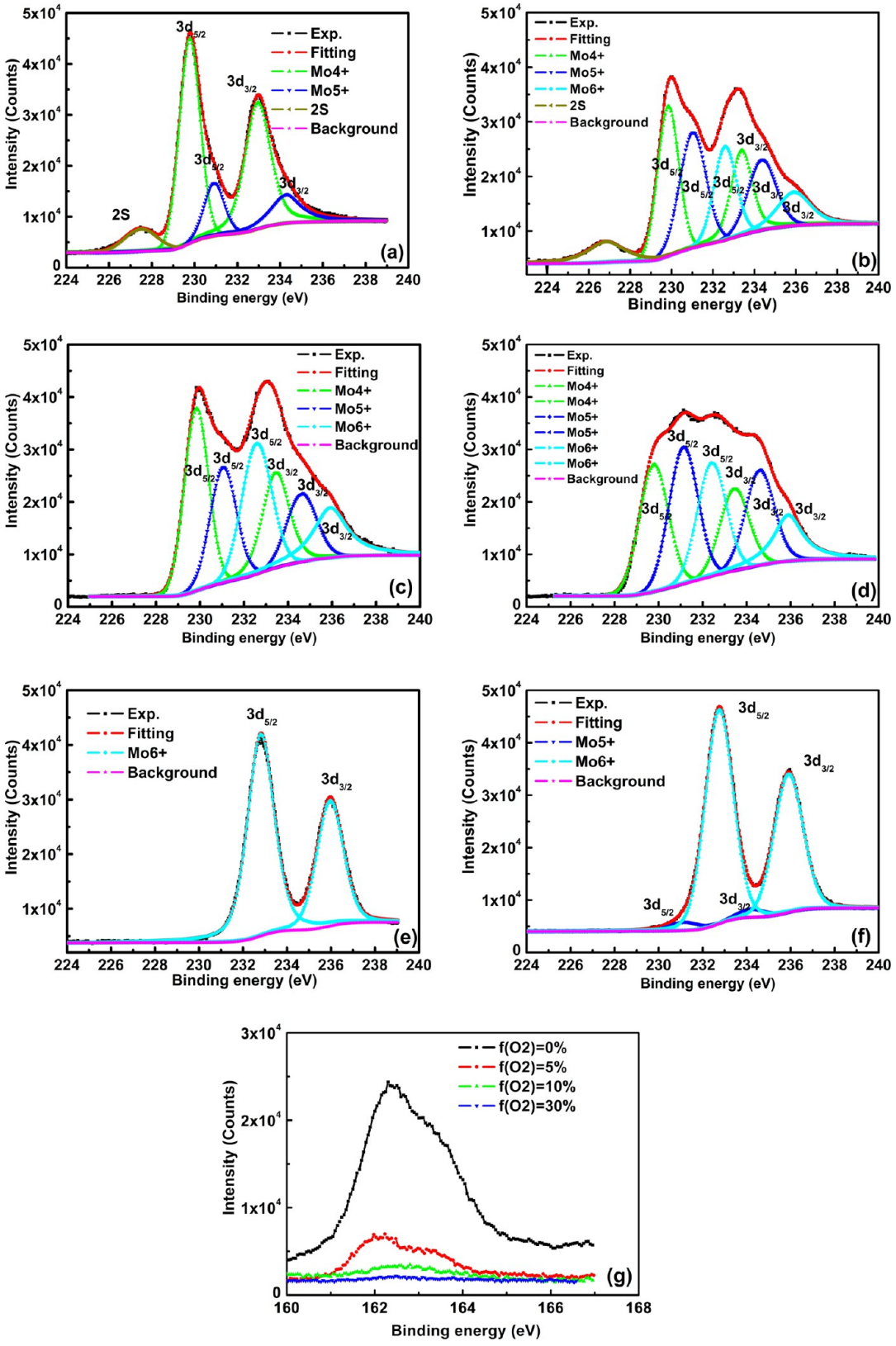

Figure 1. XPS spectra of the Mo 3d core level peaks observed for S-MoO_3 films deposited on ITO substrate with different f(O_2) at 423 K: (a) 0, (b) 5, (c) 10, (d) 20, and (e) 30%, and (f) referenced MoO_3 film. (g) XPS spectra of the S 2p core level peaks.

RESULTS AND DISCUSSION

S-MoO_3 films are formed by a RF magnetron sputtering system using a ceramic MoS_2 target in various oxygen atmospheres. To study the surface change S-MoO_3 films, XPS analysis was performed on the samples on ITO substrate with $f(O_2)$ = 0, 5, 10, 20, and 30% (Figure 1a–e) at 423K. The XPS spectra have been fitted by Gaussian-Lorentzian curves corresponding to peaks of Mo 3d. The relative contents of the various valence

dx.doi.org/10.1021/am405571a | ACS Appl. Mater. Interfaces 2014, 6, 2963–2973

Table 1. Summary of XPS Analysis of Valence States, Peak Position, and Relative Content Present in S-MoO_3 Films, Which Is According to the Mo 3d Core Level Peaks[a] for the Deposited on ITO with Different f(O_2) at 423 K, and Data of the Referenced MoO_3 Films Prepared According to the Parameters in the Literature[37]

		Mo^{4+}		Mo^{5+}		Mo^{6+}		
$f(O_2)$ (%)		$3d_{5/2}$	$3d_{3/2}$	$3d_{5/2}$	$3d_{3/2}$	$3d_{5/2}$	$3d_{3/2}$	VCEP[b]
0	position (eV)	228.8	232.0	230.0	233.4			
	relative content (%)		74.5	25.5				4.26
5	position (eV)	229.8	233.3	231.0	234.2	232.5	235.8	
	relative content (%)		40.6	33.8		25.6		4.85
10	position (eV)	229.8	233.4	231.1	234.6	232.6	235.9	
	relative content (%)		39.1	27.3		33.6		4.95
20	position (eV)	229.8	233.5	231.1	234.6	232.4	235.8	
	relative content (%)		33.4	37.6		29.0		4.96
30	position (eV)					232.8	236.0	
	relative content (%)					100		6.00
MoO_3	position (eV)			231.1	234.2	232.8	235.9	
	relative content (%)			5.4		94.6		5.94

[a]The error of these peaks is ±0.2 eV. [b]VCEP represents the statistic value of the AIL cations' electro-positivity, and it is the product of valence and the corresponding content of molybdenum oxidation states.

states of molybdenum are estimated from the cover of the Gaussian curves. The spin-orbit doublet with peaks at 229.8 and 233.0 eV were consistent with the previously reported results about MoS_2,[38,39] and the spin-orbit doublet with peaks at 232.8 and 235.9 eV, associated with Mo cations in the higher oxidation state (Mo^{6+}) have been reported in the literature,[40] which agree well with the observed main peak energies in the spectra shown in Figure 1a and Figure 1e. When $f(O_2)$ = 0%, the XPS spectrum shows progressively stronger and narrower Mo^{4+} $3d_{5/2}$, Mo^{4+} $3d_{3/2}$, S^{2-} $2p_{3/2}$, S^{2-} $2p_{1/2}$, and S 2s peaks at 229.8, 233.0, 162.3, 163.6, and 227.5 eV(shown in Figure 1a and Table 1), respectively. And a dominant Mo 3d doublet is observed with a 3.2 eV spin-orbit splitting between the Mo^{4+} $3d_{3/2}$ and Mo^{4+} $3d_{5/2}$, which is in agreement with the result reported by Fang's group.[38] These suggest that MoS_2 has been formed in the film deposited with $f(O_2)$ = 0% at 423 K, whose content in the film is 74.5%. A 25.5% Mo^{5+} in the film may be oxidized to Mo_2O_5 by the oxygen atom of the ceramic MoS_2 target or the work gas during deposition. A 3.4 eV spin-orbit splitting between the Mo^{5+} $3d_{3/2}$ 231.0 and Mo^{5+} $3d_{5/2}$ 234.4 eV is bigger than 3.1 eV that reported by Greiner,[19] which could be due to the generation of some oxygen deficiencies.

The study of density functional theory has indicated MoS_2 is highly susceptible to oxidation by atomic oxidation, and the lower coordinated Mo sites are more susceptible to oxidation than the more highly coordinated Mo sites.[41] With the oxygen content in the work gas during deposition increasing to 5%, there are three molybdenum oxidation states. And the narrower doublet Mo 3d peaks at 229.8 and 233.3 eV correspond to Mo^{4+} $3d_{5/2}$ and Mo^{4+} $3d_{3/2}$ peaks (Figure 1b). And there is ca. 0.8 eV for S 2s peak (226.7 eV) to shift to lower binding energy. However, the intensity of S 2p peak decreases (Figure 1g). This shows that Mo^{4+} peaks belong to MoS_2, and its content decreases to 40.6%. The broader Mo 3d peaks at 231.0, 234.2, 232.5, and 235.8 eV correspond to Mo^{5+} 3d and Mo^{6+} 3d peaks, which belongs to MoO_x and the contents are 33.8 and 25.6%, respectively. These indicate that part of MoS_2 decomposes to MoO_x. With $f(O_2)$ increasing to 10%, broader and broader Mo 3d peaks can be observed considerably. The Mo 3d XPS spectrum is fitted to the doublet peaks at 229.8 and 233.4 eV, corresponding to Mo^{4+} $3d_{5/2}$ and Mo^{4+} $3d_{3/2}$ peaks. The peaks at 231.1 and 234.6 eV are corresponding to Mo^{5+} $3d_{5/2}$ and Mo^{5+} $3d_{3/2}$ peaks, and the doublet peaks at 232.6 and 235.9 eV belong to Mo^{6+} with the spin-orbit splitting increasing to ca. 3.5 eV, which reveals that there are three molybdenum oxidation states, 39.1% Mo^{4+}, 27.3% Mo^{5+}, and 33.6% Mo^{6+} in the film (Figure 1c). It is worthwhile to note that the intensity of S 2p peak decreases drastically (Figure 1g). This is shown that most MoS_2 decompose to MoO_2, and a small amount of sulfur has been doped in the MoO_x film. When $f(O_2)$ = 20%, the component of sulfur decrease further, and Mo^{4+} and Mo^{6+} decrease to 33.4 and 29.0%, respectively. However, Mo^{5+} increases to 37.6%, which is related to oxygen deficiencies[19] and could result in more serious distortion in the mixed-valent molybdenum film. When further increase $f(O_2)$ to 30%, XPS analysis shows that the Mo^{6+} is the dominant oxidation state with a dominant Mo 3d doublet observed with a 3.2 eV spin-orbit splitting between Mo^{6+} $3d_{5/2}$(232.8 eV), and Mo^{6+} $3d_{3/2}$ (236.0 eV) bands, which agrees well with the Mo^{6+} species characteristic of stoichiometric MoO_3 [40] (Figure 1e). In this case, it is difficult to find the characteristic peak of S 2p (Figure 1g), and thus MoS_2 and MoO_2 are almost oxidized completely to MoO_3. Therefore, the modulation of the constituent of molybdenum oxides by sulfur doping can be achieved with controlling f(O_2) during deposition. In other words, the electronic properties of S-MoO_3 film could be tuned by sulfur doping, which could affect the properties of OSC used S-MoO_3 as AIL.

A referenced MoO_3 film prepared according to the literature[37] was analyzed by XPS too (Figure 1f). It is found that two molybdenum oxidation states, Mo^{5+} and Mo^{6+}, exist in the film, and the peaks are at 231.1 (Mo^{5+} $3d_{5/2}$), 234.2 (Mo^{5+} $3d_{5/2}$), 232.8(Mo^{6+} $3d_{3/2}$), and 235.9(Mo^{6+} $3d_{3/2}$) eV, respectively. The Mo 3d doublets are observed with a 3.1 eV spin-orbit splitting between the Mo $3d_{3/2}$ and Mo $3d_{5/2}$ bands (Table 1), which is in agreement with the results reported by Greiner[19] and Wagner.[40] The electronic band structure of MoO_3 is highly dependent on the molybdenum cation oxidation states.[42] The dominant defect in MoO_3 is oxygen vacancies, as a result of thermodynamic requirements, which causes Mo^{5+} cations to form in the film. Certainly Mo^{5+} cations are also present because of a non-zero concentration of O-vacancies.[19] MoO_2 is the lowest stable molybdenum oxide, and

it contains Mo^{4+} cations. But here, its characteristic peaks are not found in the XPS spectra.

The WF is a property that is difficult to control due to its extreme sensitivity to a number of factors, such as surface defects, chemical state and the presence of adsorbates.[42] The transition-metal oxide film is a multivalent complex. Then, the multiple cation oxidation states have a great influence on its WF. Figure 2 is the UPS spectra of S-MoO_3 and MoO_3 films,

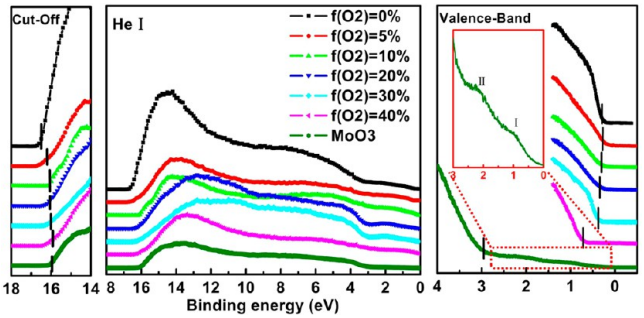

Figure 2. UPS spectra of S-MoO_3 film on ITO substrate. The full UPS spectra using He I radiation (center), secondary-electron cutoff (left), and the valence-band region (right) are included. The inset in the valence-band region (right) is the expanded view of shallow valence features. The gap state resulting from the oxygen vacancy defects is labeled I and II. A referenced MoO_3 film was also prepared according to the parameters in the literature.[37]

and the left shows the spectra of secondary electron cut-off that are used for determining WF (Table 1). Kim's group reported that MoS_2 has the WF of 4.36−4.52 eV.[43] In our work, the WF of MoS_2 film deposited with $f(O_2)$ = 0% at 423K shows a bigger WF of 4.70 eV. This may be due to the presence of molybdenum oxidation state Mo^{5+} in the film.

The increasing of WF is likely the result of the different crystal structure and high electro-positivity cation in the sample. When $f(O_2)$ = 5%, the WF of S-MoO_3 is 5.00 eV. As $f(O_2)$ increases, sulfur atom decreases (Figure 1g), low-valence-state MoS_2 is decomposed, and some molybdenum is oxidized to higher valence state cations Mo^{5+} and Mo^{6+}. These result in the slight increase of the WF of the S-MoO_3 films, which could be seen as the results of the constituent of molybdenum oxides modulated by sulfur doping. When $f(O_2)$ = 40%, MoO_3 fully occupies the sample, and it is difficult to find the peak of S 2p. And the film's WF increases to 5.24 eV, which is according to 5.20 eV reported by Hammond.[18] For the referenced MoO_3 film, WF of 5.18 eV is lower that of the S-MoO_3 film deposited with $f(O_2)$ = 40%, because 5.4% of low-oxidation-state Mo^{5+} cations exists in the film. These results show that small changes in stoichiometry give rise to significant changes in WF. Therefore, it is concluded that sulfur doping can modulate the constituent of molybdenum cations, whose electro-positivity can affect the WF of films. And the higher-oxidation-state cations possess higher electro-positivity, and the corresponding film has greater WF. However, occupied defect states within the band-gap that act as donor levels affect the Fermi level position,[42] but there are no data to certify this conclusion.

The expanded valence spectra are shown in the right of Figure 2. Stoichiometric MoO_3 contains only Mo^{6+} cations, and its valence band maximum is mainly composed of O 2p states.[44] The O 2p band can be clearly distinguished in all UPS spectra, centered at ∼4.0 eV. The shallow valence features are shown in the inset of Figure 2. There are two distinct gap-state features, labeled I and II. These states are known to arise in MoO_3 with O-deficiency, becaue of electrons occupying the metal d-band.[19] When Mo^{6+} is reduced, excess electrons move into the low-lying Mo 4d orbitals,[45] and give rise to donor states within the MoO_3 band gap. Then, O-vacancy defects cause Mo^{5+} to appear, which results in the peak centered at ∼0.9 eV (binding energy) in the valence-band photoemission spectra (labeled I). After a certain vacancy concentration, Mo^{4+} cations begin to form (labeled II), which leads to the peak centered at ∼2.1 eV (binding energy). These are shown that the oxygen vacancies cause Mo^{5+} and Mo^{4+} cations to form in MoO_3, and result in a partially occupied Mo 4d-band within the MoO_3 band gap. These gap states act as n-type dopants and push MoO_3's Fermi level very close to the conduction band minimum.[19,42] Therefore, MoO_3 film was made into an n-type semiconductor.

S-MoO_3 film is a multivalent complex with Mo^{4+}, Mo^{5+}, and Mo^{6+} states, its valence band maximum is at binding energies ranging from about 0.2 to 0.7 eV. Mo^{5+} and Mo^{4+} cation states have a large proportion, and are not seen as the defect states existed in the films. Mo^{4+} state is made up of MoO_2 and MoS_2. The valence band of MoO_2 is composed of O 2p states with some mixing with the Mo 4d states.[44] Especially, Mo 4d orbitals are the mainly parts of its valence band maximum. The top of the valence band in MoS_2 consists of Mo 4d- and S 2p- type contributions.[46,47] The Mo 4d band of Mo^{5+} resulted from O-vacancy defects has also contribution to valence band of the complex. Then, these orbitals overlap interrelation can pull valence band close to S-MoO_3's Fermi level. Thus, S-MoO_3 film shows a p-type conductive characteristic. For S-MoO_3 films deposited with $f(O_2)$ = 30−40%, their major constituent is MoO_3, which also shows the p-type conductive mechanism. Therefore, metal cations and sulfur have the dominating influence on the mixed molybdenum film's WF, and can tune the WF of this compound.

Figure 3a shows the transmittance for the ca. 20 nm S-MoO_3 films deposited with different $f(O_2)$ at 423K , along with the spectrum for a 10 nm MoO_3 film used as a reference. These thicknesses of the films were obtained by optimized performance in OSCs with them as AILs. All of the films are semitransparent that can be observed by naked eyes. The MoS_2 film can be obtained with $f(O_2)$ = 0%, and it exhibits a transmittance of 23% in the range of 330−400 nm, and the transmittance increases almost linearly from 400 to 800 nm. At 800 nm, the transmittance of the MoS_2 film is about 60%. When the $f(O_2)$ increases from 5 to 40%, the transmittance of the films also increases, and the films are more than 70% transparent across the entire visible and NIR spectra. As expected, the film deposited with $f(O_2)$ = 40% shows the highest transmittance (84% in the range of 440−800 nm). All of the S-MoO_3 films are more transparent than the MoO_3 film in the wavelength range from 300 to 390 nm, and the wavelength range between 490 and 690 nm, the film S-MoO_3 deposited with $f(O_2)$ = 40% is also more transparent than the MoO_3 film. These results suggest that S-MoO_3 film is a promising AIL candidate of OSC in terms of its transmittance.

Quantitative values of band-gap energy (E_g) are evaluated using the relation[48]

$$\alpha = \frac{A}{h\upsilon}(E - E_g)^n \quad (1)$$

Where A is the band edge constant, $h\upsilon$ is the incident photon energy, and the exponent n depends on the kind of optical

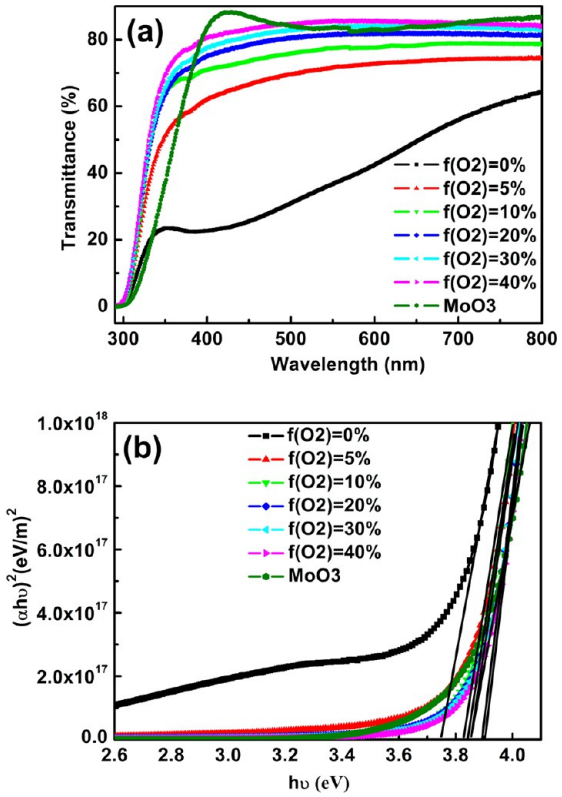

Figure 3. (a) Transmission spectra and (b) the dependence of $(\alpha h\upsilon)^2$on $h\upsilon$ for the S-MoO_3 films deposited with different f(O_2) at 423 K. The thickness of these thin films is ca. 20 nm.

transition. For crystalline materials, n can take values 1/2, 3/2, 2, or 3 for direct allowed, direct forbidden, indirect allowed and indirect forbidden transitions, respectively.[48] The best linear fit for $(\alpha h\upsilon)^2$ versus $h\upsilon$ curve is obtained for n = 1/2 for all films indicating a direct allowed transition in these films. Figure 3b presents the variation of $(\alpha h\upsilon)^2$ versus $h\upsilon$ for the S-MoO_3 films deposited at different $f(O_2)$, along with the MoO_3 film. The optical E_g has been evaluated by extrapolating the linear portion of the curve to the energy axis and the corresponding values with respect to the substrate temperature are given in Table 2. The direct band-gap of the S-MoO_3 films increases from 3.75 to 3.91 eV with $f(O_2)$ increasing from 0 to 40%. This result is consistent with the variation of transmittance of the S-MoO_3 films. This indicates that sulfur doping can tune the band gap of MoO_3.

Table 2. Summary of the energy level landscape determined from UPS (He I) and optical absorption spectra for S-MoO_3 films deposited with different f(O_2) at 423K. And a referenced MoO_3 film was prepared according to the parameters in the literature [37] in this study. The notations in the table E_g , WF , IE, IE_{GS}, and EA, denote the electronic band-gap, work function, valence band ionization energy, sub-gap state ionization energy (IE), and electron affinity (EA), respectively. The value of EA is obtained from E_g and IE

f(O_2) (%)	E_g (eV)	WF (eV)	IE (eV)	IE_{GS}(eV)	EA (eV)
0	3.75	4.70	4.97		1.22
5	3.84	5.00	5.27		1.43
10	3.86	5.11	5.40		1.54
20	3.89	5.10	5.45		1.56
30	3.90	5.15	5.52		1.62
40	3.91	5.24	5.96		2.05
MoO_3	3.85	5.18	8.12	6.13/7.24	4.27

Although the E_g of single layer MoS_2 is known to be 1.8 eV for direct type, the bulk MoS_2 has recently been reported to exhibit an indirect band-gap of ~0.6−1.3 eV.[47,49−52] So n can take value 2 for indirect allowed transitions, the band-gap from the curve of $(\alpha h\upsilon)^{1/2}$ versus $h\upsilon$ for MoS_2 film (not show here) is 0.8 eV, which is in accordance with the theoretical study.[47,49−52] For direct allowed transitions, the E_g is 3.75 eV, which is the cause that molybdenum oxidation states exist in the film. For MoO_3 film, 3.85 eV band-gap is smaller than that of the S-MoO_3 films with deposition condition $f(O_2)$ = 10−40%. From the above analysis of optical properties, S-MoO_3 and MoO_3 thin films both satisfy transparency requirement of AILs for OSCs.

Figure 4 shows the AFM images and the square average roughness (RMS) of S-MoO_3 films deposited on ITO with different $f(O_2)$ at 423 K. And the RMS of MoS_2 film with $f(O_2)$ = 0% is 6.59 nm. After 5% oxygen gas was introduced into chamber, its RMS decreases to 4.40 nm. When f(O_2) increases from 10 to 30%, RMS of S-MoO_3 films slightly increases from 4.49 to 4.64 nm. This is indicated that the films become much smoother with O_2 introduced into chamber during deposition. The RMS of the referenced MoO_3 film is 4.27 nm. Although the major constituent of S-MoO_3 film is MoO_3, its RMS is bigger than that of the referenced one. It is suggested that the structure and topography of MoO_3 film can be changed by sulfur doping, which may significantly affect the properties of the film and their corresponding OSCs.

A normal structure of the conventional OSC that employs P3HT as the donor and PCBM as the acceptor material is ITO/AIL/P3HT:PCBM/Al. The energy level diagram of the cell is depicted in Figure 5. It is expected that charge carriers are transported to the opposite electrodes at the interlayer from this diagram. The Fermi level of S-MoO_3 films deposited with different $f(O_2)$ is close to the valence band of the films, as shown in Figure 5. And it can be inferred that these films serve as p-type semiconductor. However, the Fermi level of the MoO_3 film prepared by RF according to the literature[37] is near its conduction band, and exhibits n-type conductivity. And the n-type film with deep energy levels could achieve hole selectivity by its gap states below the Fermi level, not its valence band.[24] As noted above, the films deposited by the above two methods were chosen as the AILs of OSCs. The J−V curves of OSCs are presented in Figure 6, and their photovoltaic performance is summarized in Table 3.

An open-circuit voltage V_{OC} of 0.511 V, a short-circuit current density J_{SC} of 6.33 mA/cm^2, a fill factor FF of 33.5%, and a corresponding PCE of 1.08% are obtained from the OSC used MoS_2 deposited with $f(O_2)$ = 0% at 423 K as AIL. When S-MoO_3 film has been deposited with $f(O_2)$ = 5%, the corresponding V_{OC}, J_{SC}, FF, and PCE of OSC are improved to 0.619 V, 8.31 mA/cm^2, 58.0%, and 2.98%. The OSC with S-MoO_3 film deposited with $f(O_2)$ = 10% has better performance. And the PCE of 3.69% is recorded for the device with V_{OC} 0.630 V, J_{SC} 10.05 mA/cm^2, and FF 58.3%. With $f(O_2)$ increasing from 20 to 40%, the properties of OSCs show relatively poor performance, and there is a small decrease in V_{OC} from 0.630 to 0.619 V, J_{SC} decreases from 10.05 to 9.67 mA/cm^2, and FF changes very little. For the OSC used MoO_3 as AIL, the V_{OC}, J_{SC}, FF, and PCE is 0.613 V, 9.68 mA/cm^2,

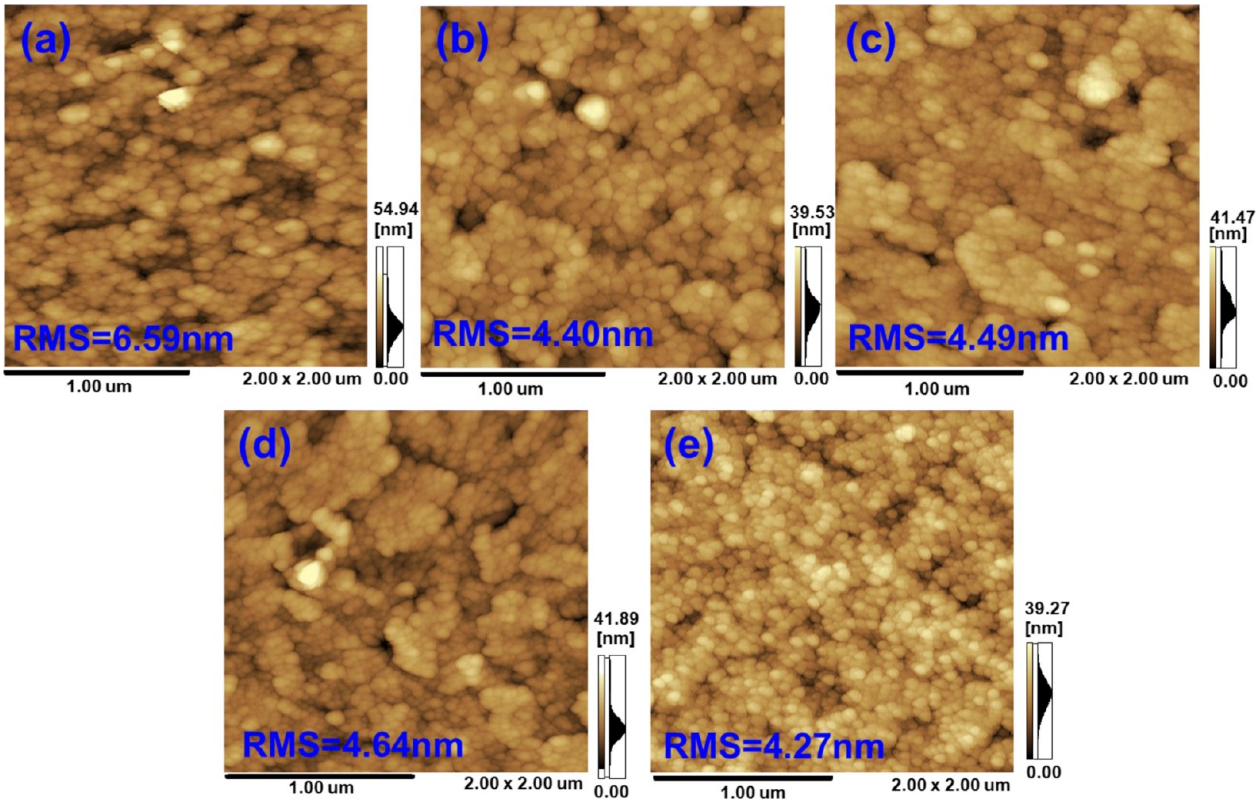

Figure 4. AFM images and the square average roughness (RMS) of S-MoO_3 films deposited on ITO substrate with different f(O_2) at 423 K: (a) 0, (b) 5, (c) 10, and (d) 30%, and (e) referenced MoO_3 film. The thickness of these films in the samples is ca. 100 nm.

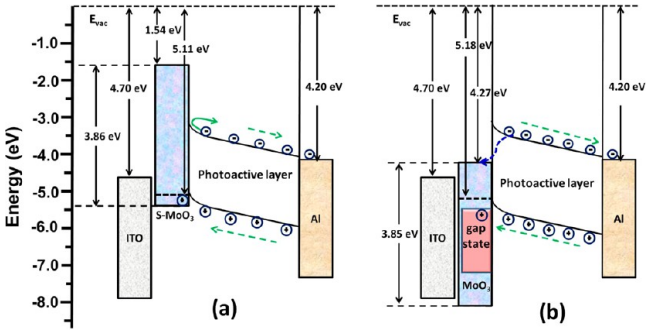

Figure 5. Schematic energy level diagrams of device components referenced to the vacuum level. (a) S-MoO_3 film deposited with $f(O_2)$ = 10%, (b) MoO_3 film prepared according to the parameters in the literature.[37]

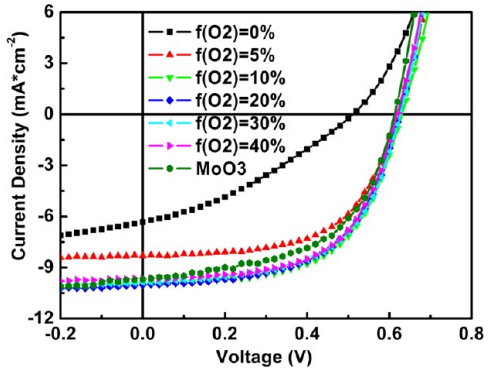

Figure 6. The illuminated J–V characteristics of the OSCs used S-MoO_3 films (ca. 20 nm) as AILs deposited with different $f(O_2)$ at 423 K. Olive hexagon line denotes the illuminated J–V characteristic of device using 10 nm MoO_3 film as AIL .

55.2%, and 3.28%, respectively, which is lower than those of the OSC with S-MoO_3 as AIL deposited with $f(O_2)$ = 10–40%, which could result from sulfur doping.

It has been reported that the V_{OC} is governed by HOMO of donor and the lowest unoccupied molecular orbital (LUMO) levels of acceptor,[4,53] which can't be used to explain the enhancement of V_{OC} in our case. The large WF of AIL is expected to induce spontaneous charge transfer from an organic semiconductor to AIL, in accordance with the charge transfer theory.[54,55]

The low charge extraction barriers at the AIL/PAL interfaces are believed to be a result of favorable energy level alignment between AIL and organic semiconducting molecules. This is a result of the AIL's deep electronic energy levels and high WF value that allow facile charge transfer from the HOMO of an organic molecule to the anode. The high V_{OC} suggests a good band alignment between PAL and the electrodes, and the slightly lower V_{OC} is obtained because of mismatched WF between MoS_2 and PAL.[43] From UPS and band-gap results, MoS_2 thin-films are not suitable for interfacial layers due to WF values that are slightly mismatched with P3HT (or PCBM) and band-gap values that is small for a direct band-gap of single-layer MoS_2 (1.8 eV) or an indirect band-gap of bulk MoS_2 (1.2 eV).[56] As $f(O_2)$ increases, higher electro-positivity cations exist in these films, which can increase the mixed oxide molybdenum films' WF. Then, the V_{OC} of corresponding OSC increases too. With $f(O_2)$ increasing from 0 to 40%, the lower-valence-state molybdenum is oxidized to higher-valence-state one, and the VCEP (VCEP represents the statistic value of the AIL cations'

dx.doi.org/10.1021/am405571a | ACS Appl. Mater. Interfaces 2014, 6, 2963–2973

Table 3. Device Operation Parameters for Devices Using S-MoO_3 films (ca.20 nm) as AILs Deposited with Different $f(O_2)$ at 423 K in This Study[a]

$f(O_2)$ (%)	R_S (Ω cm^2)	R_p (Ω cm^2)	V_{oc} (V)	J_{sc} (mA/cm^2)	FF (%)	PCE (%)
0	55.4	267	0.511	6.33	33.5	1.08
5	15.9	861	0.619	8.31	58.0	2.98
10	16.0	1881	0.630	10.05	58.3	3.69
20	16.2	769	0.625	10.01	57.9	3.62
30	13.0	554	0.625	9.86	58.0	3.57
40	17.0	408	0.619	9.67	58.1	3.48
MoO_3	19.5	400	0.613	9.68	55.2	3.28

[a]A reference solar cell with ca.10 nm MoO3 as AIL was fabricated. There are 20 samples for each device, and there are about 140 samples prepared in this study. The errors of PCEs are ±0.22%.

electro-positivity, and it is the product of valence and the corresponding content of molybdenum oxidation states.) keeps an increasing trend from 4.26 to 6.00 (Table 1), which leads to the slight increase in the WF of the S-MoO_3 films and the higher V_{OC} of OSC. However, when S-MoO_3 film is deposited with $f(O_2)$ = 40%, the corresponding V_{OC} decrease to 0.619 V.

The proper amount metal cation can affect the properties of OSC. The proper amount of Mo^{5+} existed in S-MoO_3 film is benefited to charge transfer. We suspect the excessive Mo^{5+} could increase the charge extraction barriers that result from more serious distortion and vacancies in the mixed molybdenum film. At $f(O_2)$ = 20%, 37.6% Mo^{5+} may be excessive for the S-MoO_3 film as AIL of OSC. The serious distortion could play a scattering effect during hole-transferring, and increase the contact resistance at the interface of AIL/PAL (or anode/AIL), which can reduce its ability of collecting hole and share the V_{OC} of OSC. As a result, the V_{OC} and J_{SC} of OSC decrease to 0.625 V and 10.01 mA/cm^2, respectively.

Phase segregation of donor towards anode and acceptor towards cathode in OSCs can offer the advantages of efficient charge transport and enhanced electrode selectivity,[57,58] which can effectively decrease current leakage or avoid electrical shorts to improve properties of OSC. Specifically, it is desirable for OSC that a series resistance (R_s) (defined by $R_s = [\Delta V/\Delta J]_{J=0}$, calculated from $J-V$ characteristics) approaches zero and a shunt resistance (R_p) (defined by $R_p = [\Delta V/\Delta J]_{V=0}$, calculated from $J-V$ characteristics) approaches infinity.[59,60] Besides annealing treatment, the substrate with AIL has a great impact on the vertical phase segregation of PAL.[58] The proper amount sulfur existed in the films exhibits inevitably the affinity with the sulfonic acid groups of P3HT, which benefits the phase vertical separation of PAL[61] to improve the device characteristics including V_{OC}, the shunt resistance and FF of OSC. And excessive or too small amount of sulfur cannot get this function. Sulfur doping has almost no effect on R_s of OSCs. But, when $f(O_2)$ increases from 0 to 10%, the sulfur in the film decreases sharply, and the R_p of OSCs increases from 267 to 1881 Ω cm^2. The bigger R_p is suggested that the phase separation of PAL is better, and the corresponding OSCs show better properties. With $f(O_2)$ increasing further, the sulfur characteristics in XPS spectra vanishes (Figure 1g). And the R_p decreases and the corresponding OSCs show poor properties. So the proper amount sulfur existed in the films could affect the properties of OSC. When $f(O_2)$ = 10%, the corresponding OSC shows the biggest V_{OC}, R_p, and FF with proper amounts of sulfur existed in AIL (Table 3).

Figure 7 shows the plots of the incident photon conversion efficiency (IPCE) spectra versus the wavelength of the incident

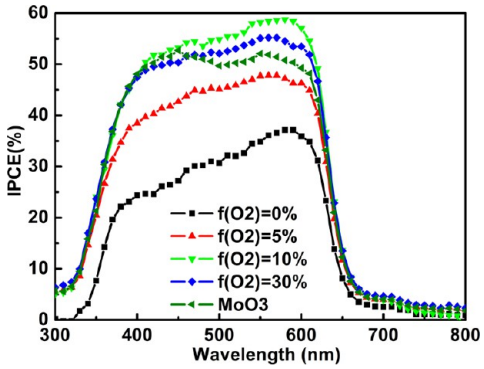

Figure 7. IPCE spectra of the devices using S-MoO_3 films (ca. 20 nm) as AILs deposited with different $f(O_2)$ at 423 K in this study. Olive prism line represents the IPCE characteristic of the referenced OSC using MoO_3 (ca. 10 nm) as AIL.

light for the devices used S-MoO_3 films as AILs. The IPCE of the referenced device using MoO_3 film as AIL is also shown here. We can see that all OSCs have an increased IPCE in the 330−680 nm. When $f(O_2)$ decreases, more and more MoS_2 may exist in the film. MoS_2 film has ca. 1.2 eV band-gap,[43,62,63] which is not suitable as a AIL of conventional OSC. However, the MoS_2 film obtained with $f(O_2)$ = 0% exhibits the transmittance with increasing linearly from in the range of 400-800 nm, the corresponding OSC shows the photovoltaic properties, and its IPCE also increases linearly from 22 to 37% in the range of 370−600 nm. For $f(O_2)$ = 5%, the IPCE also shows the characteristic with increasing linearly, and the corresponding J_{SC} increases to 8.31 mA/cm^2. The maximum IPCE is about 60% at 600 nm for the OSC with S-MoO_3 film deposited with $f(O_2)$=10% at 423 K, and the J_{SC} is the biggest 10.05 mA/cm^2, which also demonstrated that the proper amount metal cation and sulfur can cause more effective hole-transporting for improving the solar cell performance. When the $f(O_2)$ increases further, the IPCE decreases, the J_{SC} decreases accordingly to 9.86 mA/cm^2. It is concluded the J_{SC} change agrees with the IPCE of the fabricated devices. Besides that the IPCE is related with the absorption of PAL, it is also affected by the optical properties of AIL.

For p-type semiconductor S-MoO_3 films, there is no sub-gap states found at the valence band edges (shown in the right of Figure 2). Hole-transfer through the valence band can effectively avoid the recombination with electron. And the smaller EA (higher conduction band) could make them for better electron blocking (Figure 5). Therefore, J_{SC} of the reference OSC is lower than that of OSC with S-MoO_3 as AIL. MoO_3 is n-type conductivity (its Fermi level is near the conduction band (Figure 5b) originated from intrinsic oxygen vacancies that is too small to be accurately determined by XPS/UPS. Then, the two sub-gap states (at 6.13 eV and 7.24 eV) at the valence band edges participates in hole transfer,[19,24,42] and the conduction band of MoO_3 can effectively assist in recombination of photo-generated charges in the absence of the electron limiting barrier. Instead electrons are transported from ITO to the MoO_3/organic interface through MoO_3 gap states with subsequent recombination with holes. For the conduction band of MoO_3, it is too low to block electrons and to effectively avoid the recombination of photo-generated

charges. Although the WF of MoO_3 prepared by us according to the fabrication conditions of literature[37] is almost the same as that of S-MoO_3 films deposited with $f(O_2)$ = 10−40%, J_{SC} of the reference OSC is lower than that of OSC with S-MoO_3 as AIL. Therefore, S-MoO_3 is better suitable as an efficient AIL.

CONCLUSIONS

In summary, S-MoO_3 films by RF sputtering and OSCs with S-MoO_3 AIL have been studied. We demonstrate that $f(O_2)$ = 10% and ca. 20 nm S-MoO_3 layer are the best condition for OSC, and PCE up to 3.69% has been achieved. The WF of MoO_3 can be modulated with proper amount of metal cations and sulfur doping, and S-MoO_3 film was shown to be a p-type semiconductor. The smaller EA could better block electron, which can effectively avoid the recombination with electron when holes transfer through the valence band. It is clearly demonstrated that a simple and efficient sulfur doping into MoO_3 is a useful method to tune hole-transport properties and to further open new avenues for the modification of interfacial materials.

AUTHOR INFORMATION

Corresponding Authors

*E-mail: gjfang@whu.edu.cn. Tel: +86 (0)27 68752147. Fax: +86 (0)27 68752569 (G.F.).
*E-mail: xzzhao@whu.edu.cn (X.Z.).

Notes

The authors declare no competing financial interest.

ACKNOWLEDGMENTS

This work was supported by the China Postdoctoral Science Foundation (2013M531737), the National Basic Research Program (2011CB933300) of China, the Natural Science Foundation of Jiangsu Province (BK20131186) and Shenzhen Strategic Emerging Industry Development Funds (JCYJ20130401160028796), the Science Foundation (K201311), and the Youths Science Foundation (Q201108) of Wuhan Institute of Technology.

REFERENCES

(1) Günes, S.; Neugebauer, H.; Sariciftci, N. S. Conjugated Polymer-Based Organic Solar Cells. *Chem. Rev.* **2007**, *107*, 1324−1338.
(2) Yang, T.; Wang, M.; Cao, Y.; Huang, F.; Huang, L.; Peng, J.; Gong, X.; Cheng, S. Z. D.; Cao, Y. Polymer Solar Cells with A Low-Temperature-Annealed Sol-Gel-Derived MoO_x Film as a Hole Extraction Layer. *Adv. Energy Mater.* **2012**, *2*, 523−527.
(3) You, J.; Dou, L.; Yoshimura, K.; Kato, T.; Ohya, K.; Moriarty, T.; Emery, K.; Chen, C. C.; Gao, J.; Li, G.; Yang, Y. A Polymer Tandem Solar Cell with 10.6% Power Conversion Efficiency. *Nat. Commun.* **2013**, *4*, 1446.
(4) Scharber, M. C.; Mühlbacher, D.; Koppe, M.; Denk, P.; Waldauf, C.; Heeger, A. J.; Brabec, C. J. Design Rules for Donors in Bulk-Heterojunction Solar Cells—Towards 10 % Energy-Conversion Efficiency. *Adv. Mater.* **2006**, *18*, 789−794.
(5) Manders, J. R.; Tsang, S. W.; Hartel, M. J.; Lai, T. H.; Chen, S.; Amb, C. M.; Reynolds, J. R.; So, F. Solution-processed Nickel Oxide Hole Transport Layers in High Efficiency Polymer Photovoltaic Cells. *Adv. Funct. Mater.* **2013**, *23*, 2993−3001.
(6) Zhang, F.; Johansson, M.; Andersson, M. R.; Hummelen, J. C.; Inganäs, O. Polymer Photovoltaic Cells with Conducting Polymer Anodes. *Adv. Mater.* **2002**, *14*, 662−665.
(7) Jorgensen, M.; Norrman, K.; Krebs, F. C. Stability/Degradation of Polymer Solar Cells. *Sol. Energy Mater. Sol. Cells* **2008**, *92*, 686−714.
(8) Irwin, M. D.; Buchholz, D. B.; Hains, A. W.; Chang, R. P. H.; Marks, T. J. P-type Semiconducting Nickel Oxide as an Efficiency-enhancing Anode Interfacial Layer in Polymer Bulk-heterojunction Solar Cells. *Proc. Natl. Acad. Sci.* **2008**, *105*, 2783−2787.
(9) Shrotriya, V.; Li, G.; Yao, Y.; Chu, C. W.; Yang, Y. Transition Metal Oxides as the Buffer Layer for Polymer Photovoltaic Cells. *Appl. Phys. Lett.* **2006**, *88*, 073508.
(10) Kyaw, A. K. K.; Sun, X. W.; Jiang, C. Y.; Lo, G. Q.; Zhao, D. W.; Kwong, D. L. An Inverted Organic Solar Cell Employing a Sol-Gel Derived ZnO Electron Selective Layer and Thermal Evaporated MoO_3 Hole Selective Layer. *Appl. Phys. Lett.* **2008**, *93*, 221107.
(11) Liu, J.; Shao, S.; Fang, G.; Meng, B.; Xie, Z.; Wang, L. High-Efficiency Inverted Polymer Solar Cells with Transparent and Work-Function Tunable MoO_3-Al Composite Film as Cathode Buffer Layer. *Adv. Mater.* **2012**, *24*, 2774−2779.
(12) Zilberberg, K.; Trost, S.; Meyer, J.; Kahn, A.; Behrendt, A.; Lützenkirchen-Hecht, D.; Frahm, R.; Riedl, T. Inverted Organic Solar Cells with Sol−Gel Processed High Work-function Vanadium Oxide Hole-Extraction Layers. *Adv. Funct. Mater.* **2011**, *21*, 4776−4783.
(13) Qin, P. L.; Fang, G. J.; Sun, N. H.; Fan, X.; Zheng, Q.; Chen, F.; Wan, J. W.; Zhao, X. Z. Organic Solar Cells with p-type Amorphous Chromium Oxide Thin Film as Hole-transporting Layer. *Thin Solid Films* **2011**, *519*, 4334−4341.
(14) Stubhan, T.; Li, N.; Luechinger, N. A.; Halim, S. C.; Matt, G. J.; Brabec, C. J. High Fill Factor Polymer Solar Cells Incorporating a Low Temperature Solution Processed WO_3 Hole Extraction Layer. *Adv. Energy Mater.* **2012**, *2*, 1433−1438.
(15) Tan, Z. A.; Li, L. J.; Cui, C. H.; Ding, Y. Q.; Xu, Q.; Li, S. S.; Qian, D. P.; Li, Y. F. Solution-Processed Tungsten Oxide as an Effective Anode Buffer Layer for High-Performance Polymer Solar Cells. *J. Phys. Chem. C* **2012**, *116*, 18626−18632.
(16) Han, S.; Shin, W. S.; Seo, M.; Gupta, D.; Moon, S.; Yoo, S. Improving Performance of Organic Solar Cells Using Amorphous Tungsten Oxides as an Interfacial Buffer Layer on Transparent Anodes. *Org. Electron.* **2009**, *10*, 791−797.
(17) Tokmoldin, N.; Griffiths, N.; Bradley, D. D. C.; Haque, S. A. A Hybrid Inorganic-Organic Semiconductor Light-Emitting Diode Using ZrO_2 as an Electron-Injection Layer. *Adv. Mater.* **2009**, *21*, 3475−3478.
(18) Hammond, S. R.; Meyer, J.; Widjonarko, N. E.; Ndione, P. F.; Sigdel, A. K.; Garcia, A.; Miedaner, A.; Lloyd, M. T.; Kahn, A.; Ginley, D. S.; Berry, J. J.; Olson, D. C. A Hybrid Inorganic-Organic Semiconductor Light-Emitting Diode Using ZrO_2 as an Electron-Injection Layer. *J. Mater. Chem.* **2012**, *22*, 3249−3254.
(19) Greiner, M. T.; Chai, L.; Helander, M. G.; Tang, W. M.; Lu, Z. H. Metal/Metal-Oxide Interfaces: How Metal Contacts Affect the Work Function and Band Structure of MoO_3. *Adv. Funct. Mater.* **2013**, *23*, 215−226.
(20) Kröger, M.; Hamwi, S.; Meyer, J.; Riedl, T.; Kowalsky, W.; Kahn, A. P-type Doping of Organic Wide Band Gap Materials by Transition Metal Oxides: A Case-Study on Molybdenum Trioxide. *Org. Electron.* **2009**, *10*, 932−938.
(21) Irfan; Zhang, M.; Ding, H.; Tang, C. W.; Gao, Y. Strong Interface p-Doping and Band Bending in C60 on MoO_x. *Org. Electron.* **2011**, *12*, 1588−1593.
(22) Jasieniak, J. J.; Seifter, J.; Jo, J.; Mates, T.; Heeger, A. J. A Solution-Processed MoO_x Anode Interlayer for Use within Organic Photovoltaic Devices. *Adv. Funct. Mater.* **2012**, *22*, 2594−2605.
(23) Sun, Y.; Takacs, C. J.; Cowan, S. R.; Seo, J. H.; Gong, X.; Roy, A.; Heeger, A. J. Efficient, Air-Stable Bulk Heterojunction Polymer Solar Cells Using MoO_x as the Anode Interfacial Layer. *Adv. Mater.* **2011**, *23*, 2226−2230.
(24) Wong, K. H.; Ananthanarayanan, K.; Luther, J.; Balaya, P. Origin of Hole Selectivity and the Role of Defects in Low-Temperature Solution-Processed Molybdenum Oxide Interfacial Layer for Organic Solar Cells. *J. Phys. Chem. C* **2012**, *116*, 16346−16351.
(25) Zilberberg, K.; Gharbi, H.; Behrendt, A.; Trost, S.; Riedl, T. Low-Temperature, Solution-Processed MoO_x for Efficient and Stable Organic Solar Cells. *ACS Appl. Mater. Interfaces* **2012**, *4*, 1164−1168.

(26) Girotto, C.; Voroshazi, E.; Cheyns, D.; Heremans, P.; Rand, B. P. Solution-Processed MoO_3 Thin Films as a Hole-Injection Layer for Organic Solar Cells. *ACS Appl. Mater. Interfaces* **2011**, *3*, 3244−3247.
(27) Yao, C.; Xu, X.; Wang, J.; Shi, L.; Li, L. Low-Temperature, Solution-Processed Hole Selective Layers for Polymer Solar Cells. *ACS Appl. Mater. Interfaces* **2013**, *5*, 1100−1107.
(28) Cheng, F.; Fang, G. J.; Fan, X.; Huang, H. H.; Zheng, Q.; Qin, P. L.; Lei, H. W.; Li, Y. F. Enhancing the Performance of P3HT:ICBA Based Polymer Solar Cells Using LiF as Electron Collecting Buffer Layer and UV−Ozone Treated MoO_3 as Hole Collecting Buffer Layer. *Sol. Energy Mater. Sol. Cells* **2013**, *110*, 63−68.
(29) Jin, H.; Tao, C.; Velusamy, M.; Aljada, M.; Zhang, Y.; Hambsch, M.; Burn, P. L.; Meredith, P. Efficient, Large Area ITO-and-PEDOT-Free Organic Solar Cell Sub-Modules. *Adv. Mater.* **2012**, *24*, 2572−2577.
(30) Tao, C.; Xie, G.; Liu, C.; Zhang, X.; Dong, W.; Meng, F.; Kong, X.; Shen, L.; Ruan, S.; Chen, W. Semitransparent Inverted Polymer Solar Cells with MoO_3/Ag/MoO_3 as Transparent Electrode. *Appl. Phys. Lett.* **2009**, *95*, 053303.
(31) Cattin, L.; Morsli, M.; Dahou, F.; Abe, S. Y.; Khelil, A.; Bernède, J. C. Investigation of Low Resistance Transparent MoO_3/Ag/MoO_3 Multilayer and Application as Anode in Organic Solar Cells. *Thin Solid Films* **2010**, *518*, 4560−4563.
(32) Shao, S.; Liu, J.; Bergqvist, J.; Shi, S.; Veit, C.; Würfel, U.; Xie, Z.; Zhang, F. In Situ Formation of MoO_3 in PEDOT:PSS Matrix: A Facile Way to Produce a Smooth and Less Hygroscopic Hole Transport Layer for Highly Stable Polymer Bulk Heterojunction Solar Cells. *Adv. Energy Mater.* **2013**, *3*, 349−355.
(33) Chen, T. L.; Betancur, R.; Ghosh, D. S.; Martorell, J.; Pruneri, V. Efficient Polymer Solar Cell Employing an Oxidized Ni Capped Al:ZnO Anode without the Need of Additional Hole-Transporting-Layer. *Appl. Phys. Lett.* **2012**, *100*, 013310.
(34) Qin, P. L.; Fang, G. J.; He, Q.; Sun, N. H.; Fan, X.; Zheng, Q.; Chen, F.; Wan, J. W.; Zhao, X. Z. Nitrogen Doped Amorphous Chromium Oxide: Stability Improvement and Application for the Hole-Transporting Layer of Organic Solar Cells. *Sol. Energy Mater. Sol. Cells* **2011**, *95*, 1005−1010.
(35) Lee, H. S.; Min, S.-W.; Park, M. K.; Lee, Y. T.; Jeon, P. J.; Kim, J. H.; Ryu, S.; Im, S. MoS_2 Nanosheets for Top-Gate Nonvolatile Memory Transistor Channel. *Small* **2012**, *8*, 3111−3115.
(36) Castellanos-Gomez, A.; Barkelid, M.; Goossens, A. M.; Calado, V. E.; van der Zant, H. S. J.; Steele, G. A. Laser-Thinning of MoS_2: on Demand Generation of a Single-Layer Semiconductor. *Nano Lett.* **2012**, *12*, 3187−3192.
(37) Fan, X.; Fang, G. J.; Qin, P. L.; Sun, N. H.; Liu, N. S.; Zheng, Q.; Cheng, F.; Yuan, L. Y.; Zhao, X. Z. Deposition Temperature Effect of RF Magnetron Sputtered Molybdenum Oxide Films on the Power Conversion Efficiency of Bulk-Heterojunction Solar Cells. *J. Phys. D: Appl. Phys.* **2011**, *44*, 045101.
(38) Li, X.; Zhang, W.; Wu, Y.; Min, C.; Fang, J. Solution-Processed MoS_x as an Efficient Anode Buffer Layer in Organic Solar Cells. *ACS Appl. Mater. Interfaces* **2013**, *5*, 8823−8827.
(39) Benoist, L.; Gonbeau, D.; Pfister-Guillouzo, G.; Schmidt, E.; Meunier, G.; Levasseur, A. XPS Analysis of Lithium Intercalation in Thin Films of Molybdenum Oxysulphides. *Surf. Interface Anal.* **1994**, *22*, 206−210.
(40) Wagner, C. D.; Riggs, W. M.; Davis, L. E.; Moulder, J. F. *Handbook of X-ray Photoelectron Spectroscopy*;Muilenberg, G. E., Ed.; Perkin Elmer: Eden Prairie, MN, 1979; pp 104−105.
(41) Liang, T.; Sawyer, W. G.; Perry, S. S.; Sinnott, S. B.; Phillpot, S. R. Energetics of Oxidation in MoS_2 Nanoparticles by Density Functional Theory. *J. Phys. Chem. C* **2011**, *115*, 10606−10616.
(42) Greiner, M. T.; Chai, L.; Helander, M. G.; Tang, W. M.; Lu, Z. H. Transition Metal Oxide Work Functions: the Influence of Cation Oxidation State and Oxygen Vacancies. *Adv. Funct. Mater.* **2012**, *22*, 4557−4568.
(43) Yun, J. M.; Noh, Y. J.; Yeo, J. S.; Go, Y. J.; Na, S. I.; Jeong, H. G.; Kim, J.; Lee, S.; Kim, S. S.; Koo, H. Y.; Kim, T. W.; Kim, D. Y. Efficient Work-Function Engineering of Solution-Processed MoS_2 Thin-Films for Novel Hole and Electron Transport Layers Leading to High-Performance Polymer Solar Cells. *J. Mater. Chem. C* **2013**, *1*, 3777−3783.
(44) Scanlon, D. O.; Watson, G. W.; Payne, D. J.; Atkinson, G. R.; Egdell, R. G.; Law, D. S. L. Theoretical and Experimental Study of the Electronic Structures of MoO_3 and MoO_2. *J. Phys. Chem. C* **2010**, *114*, 4636−4645.
(45) Henrich, V. E.; Cox, P.A. *The Surface Science of Metal Oxides*; Cambridge University Press: Cambridge, U.K., 1994.
(46) Kadantsev, E. S.; Hawrylak, P. Electronic Structure of a Single MoS_2 Monolayer. *Solid State Commun* **2012**, *152*, 909−913.
(47) Li, T.; Galli, G. Electronic Properties of MoS_2 Nanoparticles. *J. Phys. Chem. C* **2007**, *111*, 16192−16196.
(48) Pankove, J. I. *Optical Processes in Semiconductors*; Dover Publications: New York, 1971.
(49) Wang, Q. H.; Kalantar-Zadeh, K.; Kis, A.; Coleman, J. N.; Strano, M. S. Electronics and Optoelectronics of Two-Dimensional Transition Metal Dichalcogenides. *Nat. Nanotechnol.* **2012**, *7*, 699−712.
(50) Pan, H.; Zhang, Y.-W. Tuning the Electronic and Magnetic Properties of MoS2 Nanoribbons by Strain Engineering. *J. Phys. Chem. C* **2012**, *116*, 11752−11757.
(51) Andersen, A.; Kathmann, S. M.; Lilga, M. A.; Albrecht, K. O.; Hallen, R. T.; Mei, D. First-Principles Characterization of Potassium Intercalation in Hexagonal 2H-MoS_2. *J. Phys. Chem. C* **2012**, *116*, 1826−1832.
(52) Splendiani, A.; Sun, L.; Zhang, Y.; Li, T.; Kim, J.; Chim, C. Y.; Galli, G.; Wang, F. Emerging Photoluminescence in Monolayer MoS_2. *Nano Lett* **2010**, *10*, 1271−1275.
(53) Dennler, G.; Scharber, M. C.; Ameri, T.; Denk, P.; Forberich, K.; Waldauf, C.; Brabec, C. J. Design Rules for Donors in Bulk-Heterojunction Tandem Solar Cells-Towards 15 % Energy-Conversion Efficiency. *Adv. Mater.* **2008**, *20*, 579−583.
(54) Gwinner, M. C.; Pietro, R. D.; Vaynzof, Y.; Greenberg, K. J.; Ho, P. K. H.; Friend, R. H.; Sirringhaus, H. Doping of Organic Semiconductors Using Molybdenum Trioxide: A Quantitative Time-Dependent Electrical and Spectroscopic Study. *Adv. Funct. Mater.* **2011**, *21*, 1432−1441.
(55) Braun, S.; Salaneck, W. R.; Fahlman, M. Energy-Level Alignment at Organic/Metal and Organic/Organic Interfaces. *Adv. Mater.* **2009**, *21*, 1450−1472.
(56) Han, S. W.; Kwon, H.; Kim, S. K.; Ryu, S.; Yun, W. S.; Kim, D. H.; Hwang, J. H.; Kang, J. S.; Baik, J.; Shin, H. J.; Hong, S. C. Band-Gap Transition Induced by Interlayer Van Der Waals Interaction in MoS_2. *Phys. Rev. B* **2011**, *84*, 045409.
(57) Arias, A. C.; Corcoran, N.; Banach, M.; Friend, R. H.; Mackenzie, J. D.; Huck, W. T. S. Vertically Segregated Polymer-Blend Photovoltaic Thin-Film Structures through Surface-Mediated Solution Processing. *Appl. Phys. Lett.* **2002**, *80*, 1695−1697.
(58) Campoy-Quiles, M.; Ferenczi, T.; Agostinelli, T.; Etchegoin, P. G.; Kim, Y.; Anthopoulos, T. D.; Stavrinou, P. N.; Bradley, D. D. C.; Nelson, J. Morphology Evolution via Self-organization and Lateral and Vertical Diffusion in Polymer: Fullerene Solar Cell Blends. *Nat. Mater.* **2008**, *7*, 158−164.
(59) Huynh, W. U.; Dittmer, J. J.; Teclemariam, N.; Milliron, D. J.; Alivisatos, A. P.; Barnham, K. W. J. Charge Transport in Hybrid Nanorod-Polymer Composite Photovoltaic Cells. *Phys. Rev. B* **2003**, *67*, 115326.
(60) Germack, D. S.; Chan, C. K.; Hamadani, B. H.; Richter, L. J.; Fischer, D. A.; Gundlach, D. J.; DeLongchamp, D. M. Substrate-Dependent Interface Composition and Charge Transport in Films for Organic Photovoltaics. *Appl. Phys. Lett.* **2009**, *94*, 233303.
(61) Kim, H.; Nam, S.; Lee, H.; Woo, S.; Ha, C. S.; Ree, M.; Kim, Y. Influence of Controlled Acidity of Hole-Collecting Buffer Layers on the Performance and Lifetime of Polymer:Fullerene Solar Cells. *J. Phys. Chem. C* **2011**, *115*, 13502−13510.
(62) Mak, K. F.; Lee, C.; Hone, J.; Shan, J.; Heinz, T. F. Atomically Thin MoS_2: A New Direct-Gap Semiconductor. *Phys. Rev. Lett.* **2010**, *105*, 136805.

(63) Yang, J.; Kim, S.; Choi, W.; Park, S. H.; Jung, Y.; Cho, M. H.; Kim, H. Improved Growth Behavior of Atomic-Layer-Deposited High-k Dielectrics on Multilayer MoS_2 by Oxygen Plasma Pretreatment. *ACS Appl. Mater. Interfaces* **2013**, *5*, 4739−4744.